AIP | Journal of Applied Physics

Self-organized one-atom thick fractal nanoclusters via field-induced atomic transport

R. Batabyal, J. C. Mahato, Debolina Das, Anupam Roy, and B. N. Dev

Citation: J. Appl. Phys. **114**, 064304 (2013); doi: 10.1063/1.4817520
View online: http://dx.doi.org/10.1063/1.4817520
View Table of Contents: http://jap.aip.org/resource/1/JAPIAU/v114/i6
Published by the AIP Publishing LLC.

JOURNAL OF APPLIED PHYSICS **114**, 064304 (2013)

Self-organized one-atom thick fractal nanoclusters via field-induced atomic transport

R. Batabyal, J. C. Mahato, Debolina Das, Anupam Roy, and B. N. Dev[a)]
Department of Materials Science, Indian Association for the Cultivation of Science, 2A and 2B Raja S. C. Mullick Road, Jadavpur, Kolkata 700032, India

(Received 10 May 2013; accepted 22 July 2013; published online 9 August 2013)

We report on the growth of a monolayer thick fractal nanostructures of Ag on flat-top Ag islands, grown on Si(111). Upon application of a voltage pulse at an edge of the flat-top Ag island from a scanning tunneling microscope tip, Ag atoms climb from the edge onto the top of the island. These atoms aggregate to form precisely one-atom thick nanostructures of fractal nature. The fractal (Hausdorff) dimension, $D_H = 1.75 \pm 0.05$, of this nanostructure has been determined by analyzing the morphology of the growing nanocluster, imaged by scanning tunneling microscopy, following the application of the voltage pulse. This value of the fractal dimension is consistent with the diffusion limited aggregation (DLA) model. We also determined two other fractal dimensions based on perimeter-radius-of-gyration (D_P) and perimeter-area (D'_P) relationship. Simulations of the DLA process, with varying sticking probability, lead to different cluster morphologies [P. Meakin, Phys. Rev. A **27**, 1495 (1983)]; however, the value of D_H is insensitive to this difference in morphology. We suggest that the morphology can be characterized by additional fractal dimension(s) D_P and/or D'_P, besides D_H. We also show that within the DLA process $D_P = D_H$ [C. Amitrano *et al.*, Phys. Rev. A **40**, 1713 (1989)] is only a special case; in general, D_P and D_H can be unequal. Characterization of fractal morphology is important for fractals in nanoelectronics, as fractal morphology would determine the electron transport behavior. © *2013 AIP Publishing LLC*. [http://dx.doi.org/10.1063/1.4817520]

I. INTRODUCTION

Controlled fabrication of nanoclusters on surfaces and their stability are important aspects in the development of nanoelectronic devices. The scanning tunneling microscope (STM) has played an important role to fabricate atomic or nanoscale structures by manipulating single atoms or molecules.[1] Field-induced nanometer- to atomic-scale manipulation on silicon surfaces has been achieved by applying voltage pulses to the STM tip.[2] The electric field from the tip causes a mass transfer (single atom or cluster) from the surface to the tip. The tip can then be moved to a predetermined surface site where the atom or the cluster can be redeposited by applying a second voltage pulse of opposite polarity.[2] Another kind of tip-pulse voltage induced mass transport has recently been observed, where the STM tip does not actually carry the mass from one point to another. One single voltage pulse at one location causes mass transport to other locations. This has been observed for Pb islands on silicon surfaces and the phenomenon has been used for building Pb nanomesas with atomic-layer precision.[3] In this case, the mass transport mechanism initially causes the formation of a monolayer (ML) thick annular ring on top of the island in a fast process and then in a slower process, apparently via vacancy diffusion from the enclosed vacancy island within the annular ring, the monolayer thick island is completed. The outer shape of the island remains unchanged during the whole process.

In this paper, we report on a novel mechanism in the STM tip-pulse voltage induced atomic migration and formation of one-atom thick fractal nanostructures. In contrast to the mechanism in Ref. 3, here, diffusion limited aggregation (DLA) appears to be responsible for the formation of fractal nanostructures. As the nanostructure grows, its shape keeps changing. We have carried out tip-pulse induced mass transport experiment on flat-top Ag islands on Si(111). The electric field associated with the voltage pulse causes the climbing of Ag atoms onto the top of the flat-top Ag island. Diffusion and aggregation of these Ag atoms on the flat-top island surface have led to a fractal structure partially covering the flat-top island. We have determined the fractal (Hausdorff) dimension of this structure. The observed value of the fractal dimension is consistent with the DLA model. To our knowledge, this is the first example of fabrication of a self-organized fractal structure using a STM. These results assume importance also for the fact that fractal structures[4] are not only of academic interest but also are useful in technological applications. "Fractal electronics" involves electronic devices fabricated using fractal structures. Fractal capacitors with submicron features, with a few times increase in the capacitance per unit area compared to standard parallel plate capacitors, have been fabricated. For these fractal capacitors, capacitance boost factors in excess of ten may be possible as the technology reaches nanoscale.[5] Antennas with fractal structures have found extensive applications in mobile telecommunications and the device size has reached mesoscale.[6–8] Applications of fractal structures in nanoelectronic devices are already being explored.[9]

[a)]Email: msbnd@iacs.res.in

For field-induced atomic transport experiment via a voltage pulse from a STM tip, the Pb/Si system was used in Ref. 3. We intended to investigate a different metal/Si system, because different adatom binding energies and diffusion activation barriers on surfaces of different metals might lead to different growth mechanisms and different self-organized structures. Earlier we investigated growth and many related interesting phenomena for the Au/Si[10–13] and the Ag/Si[14,15] systems, including fractal structure formation.[11,15] While the Au/Si system is reactive, the Ag/Si system is nonreactive like the Pb/Si system. Hence, we have chosen the Ag/Si system for the present experiment.

II. EXPERIMENTAL

The experiments were performed using a compact molecular beam epitaxy (MBE) system and a variable temperature scanning tunneling microscope (VT-STM) (Omicron Nanotechnology), operating under ultrahigh vacuum (UHV) condition with the base pressure less than 1.0×10^{-10} mbar. N-type Si (111) substrates, after proper degassing, were flashed at around 1200 °C for 45 s to obtain clean 7×7 reconstructed surfaces. The growth of Ag islands on Si (111)-7×7 surfaces is achieved by depositing Ag onto the substrates at room temperature (RT), from a Knudsen cell at the rate of 1.7 ML per min. We define a ML of Ag to be equivalent to the nominal surface atomic density of Ag(111), 1.5×10^{15} atoms/cm^2, as in Refs. 16 and 17. We have deposited 2 ML Ag, which forms percolated flat-top islands with height preferences of 2, 4, 6, … atomic layers (ALs) on a wetting layer of 1-AL as observed earlier.[16] The island surface is Ag(111).[16] This preference apparently arises from an electronic growth mode.[16,17] We applied a voltage pulse from the STM tip at the edge of a Ag island and observed time evolution of mass transport on the surface of the flat-top island via collection of successive images. STM imaging condition was +1.0 V, 0.1 nA. A voltage pulse of +7 V was applied for 1 s keeping the feed-back loop on. Then, immediately the imaging condition was brought back for collecting successive images.

III. RESULTS AND DISCUSSIONS

A. Field induced growth, growth characteristics, and fractal (Hausdorff) dimension

Fig. 1 shows a constant-current STM image (205 nm × 205 nm) of the Ag-deposited Si(111) surface. The Ag islands are flat-top and have preferred heights (not shown here) as in Ref. 16. We have chosen the island "A" in Fig. 1 for tip-pulse induced modification. This island height is equivalent to 4-AL of Ag on top of a wetting layer of 1-AL of Ag. Initially, a tip-pulse voltage of +7 volt was applied to the island "A" at the position indicated by a cross. This has produced a small hole along with a small adjacent island of adatoms as seen in Fig. 2(a). However, no major mass transport has taken place. In previous investigations on Pb islands on Si(111), major mass transport has been found to occur when the voltage pulse is applied to the tip by placing it at the edge of an island.[3,18,19] We have also found major mass

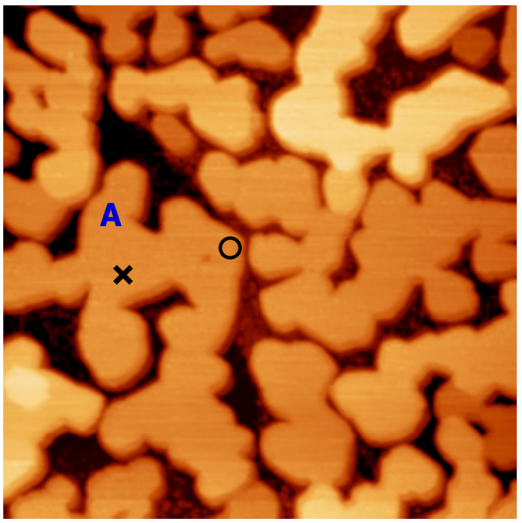

FIG. 1. A constant current ($i = 1.0$ nA, $V = 0.5$ V) STM image (205 nm × 205 nm) of a Ag thin film on a Si(111)-7×7 surface. The voltage pulses from a STM tip were applied to the positions marked by "×" and "O" on the flat-top island "A," as described in the text.

transport when the voltage pulse is applied near the island edge at the position marked by a circle in Fig. 1. Fig. 2(a), which is a part of Fig. 1, also shows this position marked by a circle. Fig. 2(b) shows the STM image taken 106 s after the application of the tip-pulse. It is readily seen that material is lost from the edge of the island and there is material accumulation on top of the island and formation of a small 1-AL thick island. Height scan along the line in Fig. 2(b), shown in Fig. 3(a), confirms this. We concentrate on the growth of this island area with time by taking successive images shown in Figs. 2(b)–2(i). The perimeter of the growing island is

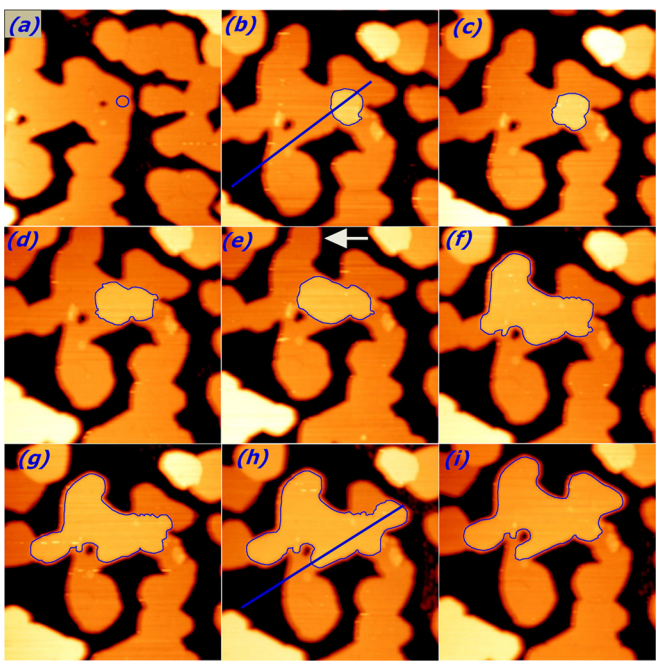

FIG. 2. (a)–(i) Constant current ($i = 0.5$ nA, $V = 0.5$ V) STM images (100 nm × 100 nm) successively taken after application of the voltage pulse at the position marked by "O" in (a). The images show the growth of a pulse voltage induced Ag island on top of the flat-top Ag island "A" in Fig. 1. The perimeter of the growing island is marked by blue lines.

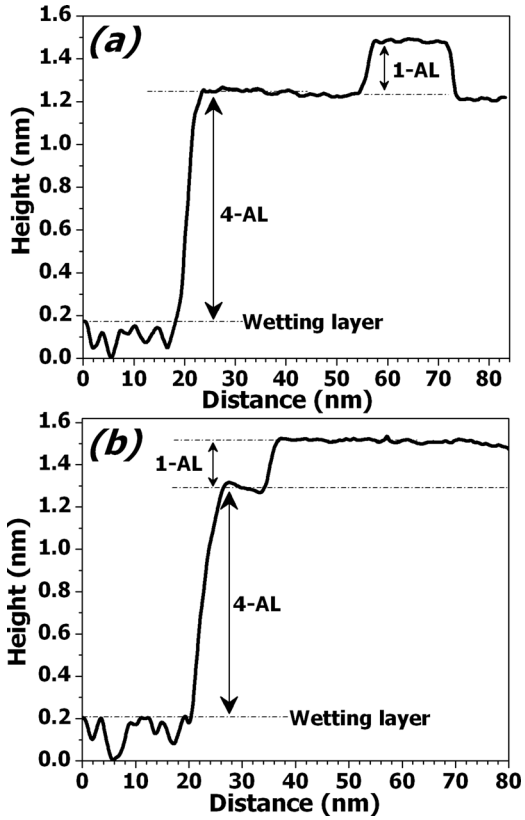

FIG. 3. (a) and (b) The height profiles along the lines marked in Figs. 2(b) and 2(h), respectively, show that the growing island is one atomic layer (1-AL) thick.

marked in Figs. 2(b)–2(i). Island area vs time plot is shown in Fig. 4. We notice an enhanced growth rate from (e) to (f) in Fig. 4. Comparing images 2(e) and 2(f), we notice that there is a massive mass transport from the region marked by the arrow in Fig. 2(e). Mass transport from other regions of island edges than where the pulse is applied has also been observed earlier for Pb islands on Si(111).[20] That the island grows only laterally and the height remains one atomic layer thick is seen in the height scan from Fig. 2(h), shown in Fig. 3(b). This growth feature is different from that for the Pb/Si(111) system. The shapes of the growing one-atom thick island are clearly different from ordinary geometrical shape.

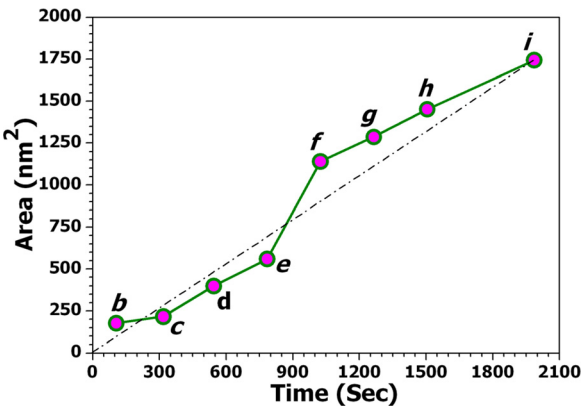

FIG. 4. The island area vs elapsed time following the application of the voltage pulse.

As we will see, these shapes belong to fractal geometry. That is, these are fractal structures.

The fractal dimension (Hausdorff dimension, D_H) of a fractal structure is defined by the cluster mass (M) scaling with the radius of gyration (R_g) as[21,22]

$$M \propto R_g^{D_H}. \quad (1)$$

In our case, the clusters are uniformly one atomic layer thick and hence the area (A) is proportional to mass (M). So,

$$A \propto R_g^{D_H}. \quad (2)$$

Usually many islands of various sizes are used for the analysis of the fractal dimension. However, for a growing island, as in the present case, if the evolution of the island can be followed, fractal dimension can be determined from a single growing island, as it is often done in simulations.[22] For the growing cluster, we have determined the area A and the corresponding R_g values[23] from the images in Fig. 2. We show the plot of ln(A) vs. ln(R_g) in Fig. 5. From the slope, we obtain $D_H = 1.75 \pm 0.05$. The measured fractal dimension is consistent with the DLA model. Theoretically, the DLA process yields a fractal dimension of about 1.7 for growth on a surface, i.e., in a 2-dimensional space.[11,22,24,25]

In order to compare the growth mechanism of the tip-pulse induced Ag island and the original Ag islands formed by Ag vapor deposition, we have also analyzed the morphology of the original Ag islands. For Ag deposition on Si(111)–(7 × 7) surfaces at RT, at low coverages, isolated Ag islands form on a wetting layer.[16,17] As the coverage is increased, percolated island structures are formed at a certain coverage. Below this percolation limit (~1.9 ML), we have carried out fractal analysis of the island structures. A STM image from the surface for a coverage of 1.8 ML Ag is shown in Fig. 6(a). We have analyzed 20 islands and found that they obey Eq. (2) indicating that they have fractal structures and the fractal dimension is found to be $D_H = 1.61 \pm 0.06$. This is shown in Fig. 6(b). The upper limit of this

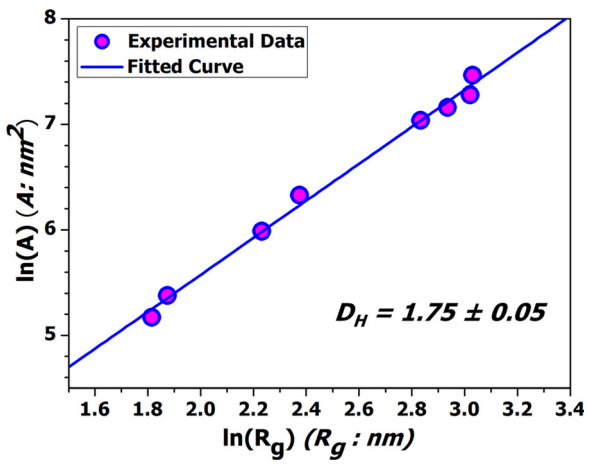

FIG. 5. The fractal dimension was obtained from the relationship between the island area (A) and the radius of gyration (R_g) from Eq. (2). Experimental ln(A) vs. ln(R_g) plot is shown. The solid line is the linear fit to the data. The slope of this line gives the fractal dimension $D_H = 1.75 \pm 0.05$.

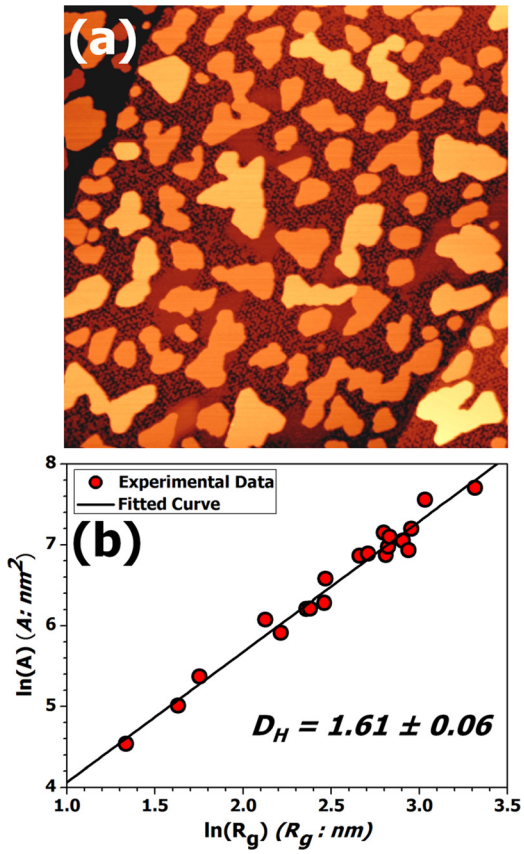

FIG. 6. (a) A 300 nm × 300 nm constant current STM image (i =0.05 nA, V = −2.1 V) showing the flat-top Ag islands onto the Si(111)-7 × 7 surface. The Ag coverage was 1.8 ML. (b) a ln(A) vs. ln(R_g) plot showing the fractal (Hausdorff) dimension D_H =1.61 ± 0.06.

value of D_H is nearly equal to the lower limit of the value of D_H obtained from the tip-pulse induced growth. The aggregation mechanism in the formation of the original Ag islands can also be identified as DLA. This is not surprising as these islands also grow on the Ag wetting layer and should follow the same diffusion and aggregation mechanism.

We could have reported STM tip-voltage induced mass transport experiment on isolated single islands, as obtained for Ag coverages below 1.9 ML. However, these islands are smaller (compared to those on the percolated structure at higher coverages) and some parts of the largest isolated island is as narrow as 10 nm. So, STM pulse induced growth of an island large enough for establishing the fractal nature could not be obtained. Radius of gyration variation at least over a decade is necessary to establish fractal scaling. That is why we have used larger islands, obtained in the percolated structure, for the investigation of STM pulse induced effects. Even on this large island, as the tip-voltage induced monolayer island grows larger, the island shape is apparently restricted by the edge of the original island. Up to the 4th point in Fig. 5, the monolayer island has not been significantly affected by any edge, yet they follow the same slope (fractal dimension) as it is for the entire range. It should be mentioned here that even the larger area of the base Ag island in percolated structure is not large enough for growing a large field-induced fractal cluster. So, the scaling relationship could not be investigated over much larger length scales. We could obtain only very limited-range fractals. In general, fractal structures with thicker branches offer the possibility of investigation of scaling behavior only over a limited range. For example, in Ref. 9, Sb island growth on highly oriented pyrolytic graphite shows thick branches and DLA fractal scaling (D_H = 1.7), where coarse cut-off length is only ~3 times the fine cut-off length. A general observation is that all fractal structures observed in recent STM growth studies are formed in the so-called extended fractal growth regime, which produces thicker branches.[26] These structures would show scaling only over a limited range length scales.

In the present experiment, we could determine neither the fine scale nor the coarse scale cut-off. If we had taken STM images at much shorter time intervals following the application of the voltage pulse, perhaps we could have determined the fine scale cut-off. The fine scale cut-off can indeed be made smaller by reducing the substrate temperature.[26] This would help increase the fractal scaling range. We could not determine or extend the coarse scale cut-off, because the growth of the field-induced Ag island was limited by the available island area on which it has been growing.

From Figs. 2(f) to 2(i), we notice that the hole on the island, created by the first pulse at "×" in Fig. 1, has not been filled by adatoms; rather the growth has proceeded by avoiding the hole on the island surface. Because of a Ehrlich-Schwoebel barrier,[27,28] atoms do not climb down the hole. For Ag diffusion on a Ag(111) surface, this barrier is 130 meV.[29] In the absence of this hole, the island perimeter and the area would have been somewhat different. We consider this difference and still find the value of the fractal dimension to be within the error bar of the determined value, as this region is only a small fraction of the total perimeter or area. The fact that the growth avoids the hole, prefabricated by STM, offers the possibility of manipulating the fractal structure to a desired form as it has been done for the fractal antenna in order to modify the behavior of the antenna.[8]

The only other case where tip-pulse voltage induced one-atom thick island formation was observed is Pb on Si(111) in Ref. 3. In contrast to the growth mechanism in the case in Ref. 3, here tip pulse induced upward atomic motion leads to the formation of a small Ag adatom island, which grows laterally in time via the DLA process. For the case of Pb island in Ref. 3, Pb atoms initially accumulate at the island edge forming an annular island and adatom diffusion on the terrace is negligible. The inner part of the annular island is filled via a vacany diffusion mechanism. Thus, the outer shape remains unchanged as the island grows. Adatom diffusion activation barrier for Ag diffusion on Ag(111) is 0.06 eV,[30] whereas this value for Pb diffusion on Pb(111) is 0.15 eV.[19] While this large difference in activation barrier could be partially responsible for the different growth behaviour, there could be other factors influencing this difference.

Electronic growth mode produces islands of preferred heights. This has been observed for Pb growth on Si(111)-(7 × 7) surfaces[31] and for Ag growth on Si(111)-(7 × 7) surfaces.[16,17,32] For Pb, the preferred island heights are 5-AL, 7-AL, 9-AL … on a wetting layer of 2-AL. Ag growth on Si(111) shows a preference for islands of 2-AL, 4-AL, 6-AL … height on a wetting layer of 1-AL.[16,17] Here, we have

applied the tip-pulse voltage on a 4-AL island, and the induced atomic migration has produced a 5-AL height island by adding one atomic layer on top of an island of 4-AL height. At RT, the 4-AL height island remains stable and the uphill transfer of Ag atoms on top of this island is apparently kinetically blocked. The triggering voltage pulse enables a large number of Ag atoms to be transferred to the top of the island, where they diffuse and aggregate. This field-assisted upward movement of Ag atoms and formation of monolayer cluster have been observed on islands of other heights than 4-AL. This feature was also observed for Pb islands, where successively applied voltage pulses have been found to add one additional atomic layer of Pb to the island.[3]

B. Other fractal dimensions and morphology of fractal structures

Fractal nature of a structure is also described by other fractal dimensions than Hausdorff dimension (D_H). Fractal dimension of the perimeter (D_P) from its dependence on R_g is defined by[22]

$$P \infty {R_g}^{D_P} \tag{3}$$

in a similar way to Eq. (1). Here, P is the length of the perimeter of the structure. The result obtained from the analysis of Fig. 2 is shown in Fig. 7. The plot in Fig. 7 yields $D_P = 1.25 \pm 0.04$.

We also investigate the morphology of the growing island via perimeter-area relationship. We measure the perimeter and the area of the island at various stages of growth. For a fractal object, the perimeter *(P)* is also related to the area (A) as[4]

$$P \infty A^{\frac{D'_P}{2}}, \tag{4}$$

where D'_P is the fractal dimension obtained from the perimeter-area relationship. The value of D'_P depends on the yardstick length (i.e., size of a pixel) used to measure P. The yardstick should be small enough[33] in order to get a reliable value of D'_P. In the present case, the yardstick value (δ) is 0.135 nm (here, $A/\delta^2 > 9000$). A ln(P) vs. ln(A) plot should be linear with a slope of $D'_P/2$. We show this plot in Fig. 8. It indeed shows the fractal nature of this growing island. The value of D'_P obtained from the plot in Fig. 8 is $D'_P = 1.43 \pm 0.05$. For a two-dimensional compact object, $D'_P = 1$.

Why have we determined various fractal dimensions? This will be clear from the discussion below. As we will see, even within the same aggregation process, say DLA, the morphology of a fractal structure can be different. In order to describe these differences in morphology, as we show below, it is necessary to have information about other fractal dimensions, in addition to the Hausdorff dimension, D_H.

The simulation of the DLA process, including the effect of diffusion via the value of sticking coefficient (S) has been carried out by Meakin.[25] From simulations for sticking coefficients $S = 1$ and $S = 0.1$, he has shown that the Hausdorff dimension (D_H) is relatively insensitive to the sticking coefficient. That is, the value of D_H remains practically constant for $S = 1$ and $S = 0.1$. However, from the simulated structures presented in Ref. 25, it is clear that the morphology of the structures for different values of S shows significant differences. For $S = 1$, the branches of the fractal structure are narrow. With decrease of the value of S, the branches become thicker, i.e., more compact. We have analyzed the structures for $S = 1$ and $S = 0.1$ (Figs. 7 and 10 in Ref. 25) and determined the value of D_H, D_P, and D'_P of those structures. We have found that while D_H is insensitive to the value of S, as reported in Ref. 25, D_P and D'_P are not. Both D_P and D'_P vary with the value of S. Thus, we suggest that the morphological differences of the fractal structures can be better described by other fractal dimensions D_P and/or D'_P in addition to the Hausdorff dimension D_H. The conclusion reached by Amitrano *et al.*[22] in their simulation of the DLA process, that $D_P = D_H$, is not apparently valid for any value of S. When the structures have more compact branches (for smaller value of S), D_P is not equal to D_H.

Our analysis from the simulated structures in Figs. 7 and 10 in Ref. 25 is shown in Table I along with the results from

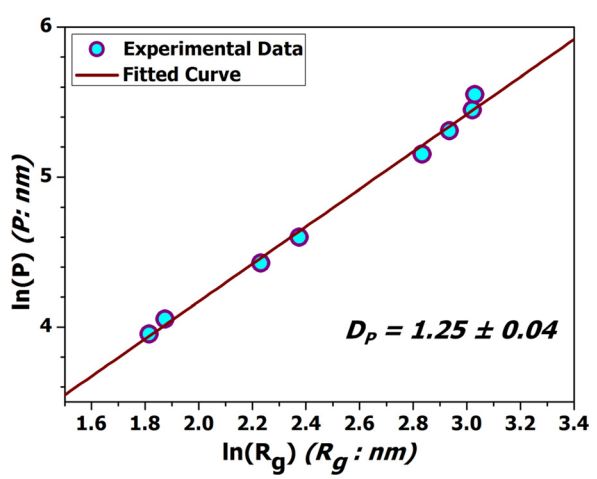

FIG. 7. The fractal dimension was obtained from the perimeter (P)–radius of gyration (R_g) relationship, Eq. (3). Experimental ln(P) vs. ln(R_g) plot is shown. The solid line is the linear fit to the data. The slope of this line gives the fractal dimension $D_P = 1.25 \pm 0.04$.

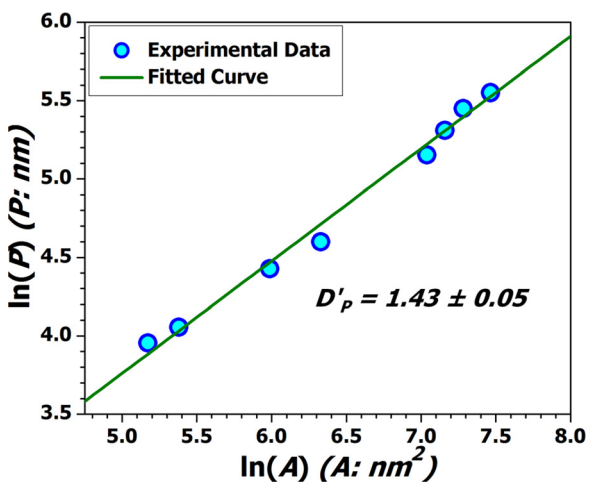

FIG. 8. The fractal dimension was obtained from the perimeter (P)–area (A) relationship, Eq. (4). Experimental ln(P) vs. ln(A) plot is shown. The solid line is the linear fit to the data. The slope of this line gives the fractal dimension $D'_P = 1.43 \pm 0.05$.

TABLE I. Values of various fractal dimensions for different sticking coefficients. In the first two rows, D_H[a] values are those given in Ref. 25. D_H, D_P, D'_P, and $D_H D'_P/D_P$ have been derived from the simulated structures in Ref. 25. The last row provides the values obtained in the present experiment. The ideal value of $D_H D'_P/D_P$ should be 2.

Sticking coefficient S	Hausdorff dimension D_H[a]	Hausdorff dimension D_H	Perimeter-area dimension D'_P	Perimeter-radius of gyration dimension D_P	Relationship between various dimensions $D_H D'_P/D_P$
1	1.71 ± 0.06	1.67 ± 0.06	2.03 ± 0.01	1.7 ± 0.05	1.99 ± 0.10
0.1	1.71 ± 0.06	1.74 ± 0.06	1.74 ± 0.14	1.52 ± 0.10	1.99 ± 0.22
Present expt.	…	1.75 ± 0.06	1.43 ± 0.05	1.25 ± 0.04	2.00 ± 0.12

the present experiment. Table I also shows a column with the value of $D_H D'_P/D_P$. From Eqs. (2)–(4), it can be shown that

$$D_H D'_P/D_P = 2. \quad (5)$$

Thus, it is not necessary to determine both D'_P and D_P. Any one of them, in conjunction with the value of Hausdorff dimension (D_H), would describe the morphology of the fractal structure better, as the value of only D_H cannot distinguish between different morphologies. The three cases shown in Table I have practically the same value of D_H; however, they have decreasing values of D'_P and D_P from top to bottom. The simulated structure in Fig. 7 of Ref. 25 for $S=1$ ($D'_P=2.03$, $D_P=1.7$) has lean branches and that in Fig. 10 of Ref. 25 for $S=0.1$ ($D'_P=1.74$, $D_P=1.52$) has more compact branches. In the present case ($D'_P=1.43$, $D_P=1.25$), the compactness of the structure has increased.

In the classic DLA model with sticking coefficient $S=1$, the average branch thickness b of the fractal island is about one atom wide ($b \approx 1$), while the fractal islands observed in vapour deposition experiments, observed by STM, have wider branch thickness.[34] These discrepancies can be removed by generalizing the DLA model to situations more appropriate to real growth systems[26] including edge diffusion and local relaxation. The authors in Ref. 26 have shown the existence of an extended fractal regime with the same fractal dimension (D_H) as in the regime of the classic DLA model. They have shown two simulations: (i) the classical DLA model (regime-I) and (ii) the extended fractal regime (regime-II). In the classical DLA model (regime-I), the average branch thickness is $b \approx 1$ and the coordination number (n_c) is peaked at 2. In regime-II, $b \approx 4$ and n_c is peaked at 5. That is, the branches are more compact. This regime-II can be compared with DLA with $S<1$. The branch thickness b increases both in regime-II in Ref. 26 and the DLA with $S<1$ in Ref. 25. Reference 26 suggests that essentially all the fractal structures observed in recent STM growth studies are formed in the extended regime (regime-II). The thickness of the branches can vary depending on the growth condition.[35] As we have proposed, the morphology of the fractal structure can be characterized by the value of D_P and/or D'_P in addition to D_H. In regime-I, $D_H = D_P \approx 1.7$ and in regime-II $D_H \neq D_P$, and the value of D_P can be anywhere between 1 and D_H. In regime-III (compact) of Ref. 26, $D_H=2$ and $D_P=1$.

Growth on a substrate at an elevated temperature would lead to lower sticking coefficient (smaller value of S) and enhanced edge diffusion. Consequently, the growth will be in the extended fractal regime with increasing branch width.[26] This change in morphology can be characterized by D_H, D_P, and D'_P values. Obviously, many properties of a fractal structure will depend on its morphology. Thus, these properties can be correlated with its D_H, D_P, and D'_P values.

Applications of fractal geometry to electronic devices are being explored. Conduction through DLA fractal devices has been simulated and it has been shown that fractal scaling properties generate novel, nonlinear conduction properties in response to depletion by electrostatic gates.[9] From the source-gate-drain structure within a fractal object, it is easy to understand that the response of this device would be different when the fractal branches are thicker, i.e., when D_P and D'_P values would be different in spite of D_H value being the same. In other words, when a fractal structure like that in Fig. 7 of Ref. 25 (morphology described by the fractal dimensions in the top row of Table I) is replaced by a fractal structure like that in Fig. 10 of Ref. 25 (fractal dimensions in the middle row of Table I) in the device, the response of these devices would definitely be different. The value of D_P or D'_P would impact on functional properties such as the connectivity between two islands. Thus, the functional properties can be related to a specific set of fractal dimensions.

IV. CONCLUSIONS

We have demonstrated a novel method for fabricating fractal nanostructures with atomic-layer precision via application of a voltage pulse from a STM tip on a Ag island on silicon. The fractal (Hausdorff) dimension of this fractal structure is found to be $D_H = 1.75 \pm 0.05$. This value of the fractal dimension is consistent with the DLA model. We have determined other fractal dimensions, D_P and D'_P, and elucidated their importance in describing the morphology of fractal clusters produced by the DLA process, considering the fact that the value of D_H is insensitive to the morphology. Characterization of fractal morphology is important for fractals in nanoelectronics, as fractal morphology would determine the electron transport behavior.

The fractal nanostructure, fabricated via a voltage pulse from a STM tip, may find applications in future fractal nanoelectronics.[6–8] Negative differential resistance (NDR), discovered in a tunnel diode by Esaki,[36] is utilized in modern electronic devices. Recently, we have reported observation of NDR in electron tunneling conductance in atomic-scale ultrathin (one to five atomic layers) Ag films on Si(111) and showed that the bias voltage at which NDR occurs depends on the film thickness.[31] The field-induced atomic transport

and the consequent addition of an atomic layer, as demonstrated here, would provide the tunability of properties, including NDR, of two-dimensional or fractal nanoelectronic devices.

Ag fractal structures on Ag may have other applications. As application of a voltage pulse on a previously formed field-induced island can form another fractal island on top, a multi-level fractal structure can be built up. Such structures would show metal-enhanced fluorescence in certain adsorbed molecules on them with widespread potential applications to the analytical sciences, imaging and medical diagnostics.[37]

ACKNOWLEDGMENTS

J.C.M. and D.D. were supported by CSIR Fellowship 09/080 (0674)/2009-EMR-I and 09/080 (0725)/2010-EMR-I, respectively. This work was partially supported by the IBIQuS project.

[1]D. M. Eigler and E. K. Schweizer, Nature (London) **344**, 524 (1990).
[2]I.-W. Lyo and P. Avouris, Science **253**, 173 (1991).
[3]C.-S. Jiang, S.-C. Li, H.-B. Yu, D. Eom, X.-D. Wang, Ph. Ebert, J.-F. Jia, Q.-K. Xue, and C.-K. Shih, Phys. Rev. Lett. **92**, 106104 (2004).
[4]B. B. Mandelbrot, *The Fractal Geometry of Nature* (Freeman, San Francisco, 1982).
[5]H. Samavati, A. Hajimiri, A. R. Shahani, G. N. Nasserbakht, and T. H. Lee, IEEE J. Solid-State Circuits **33**, 2035 (1998).
[6]C. Puente, J. Romeu, R. Bartolome, and R. Pous, Electron. Lett. **32**, 1 (1996); See www.fractus.com for fractal antenna technology.
[7]C. Puente, J. Romeu, R. Pous, and A. Cardama, "Multiband fractal antennas and arrays" in *Fractals in Engineering*, edited by J. L. Vehel, E. Lutton, and C. Tricot (Springer, New York, 1997).
[8]C. Puente Baliarda, C. B. Borau, M. N. Rodero, and J. R. Robert, IEEE Trans. Antennas Propag. **48**, 713 (2000).
[9]M. S. Fairbanks, D. N. McCarthy, S. A. Scoot, S. A. Brown, and R. P. Taylor, Nanotechnology **22**, 365304 (2011).
[10]K. Sekar, G. Kuri, P. V. Satyam, B. Sundaravel, D. P. Mahapatra, and B. N. Dev, Phys. Rev. B **51**, 14330 (1995).
[11]K. Sekar, G. Kuri, P. V. Satyam, B. Sundaravel, D. P. Mahapatra, and B. N. Dev, Solid State Commun. **96**, 871 (1995).
[12]K. Sekar, G. Kuri, P. V. Satyam, B. Sundaravel, D. P. Mahapatra, and B. N. Dev, Surf. Sci. **339**, 96 (1995).
[13]B. Sundaravel, K. Sekar, G. Kuri, P. V. Satyam, B. N. Dev, S. Bera, S. V. Narasimhan, P. Chakraborty, and F. Caccavale, Appl. Surf. Sci. **137**, 103 (1999).
[14]D. K. Goswami, K. Bhattacharjee, B. Satpati, S. Roy, G. Kuri, P. V. Satyam, and B. N. Dev, Appl. Surf. Sci. **253**, 9142 (2007).
[15]A. Roy, B. Sundaravel, R. Batabyal, and B. N. Dev, Thin Solid Films **520**, 5086 (2012).
[16]D. K. Goswami, K. Bhattacharjee, B. Satpati, S. Roy, P. V. Satyam, and B. N. Dev, Surf. Sci. **601**, 603 (2007).
[17]L. Gavioli, K. R. Kimberlin, M. C. Tringides, J. F. Wendelken, and Z. Zhang, Phys. Rev. Lett. **82**, 129 (1999).
[18]S.-C. Li, J.-F. Jia, X. Ma, Q.-K. Xue, Y. Han, and F. Liu, Appl. Phys. Lett. **89**, 123111 (2006).
[19]S.-C. Li, X. Ma, J.-F. Jia, Y.-F. Zhang, D. Chen, Q. Niu, F. Liu, P. S. Weiss, and Q.-K. Xue, Phys. Rev. B **74**, 075410 (2006).
[20]Y. Han, J. Y. Zhu, and F. Liu, Phys. Rev. Lett. **93**, 106102 (2004).
[21]R. M. Brady and R. C. Ball, Nature (London) **309**, 225 (1984).
[22]C. Amitrano, P. Meakin, and H. E. Stanley, Phys. Rev. A **40**, 1713 (1989).
[23]We have determined R_g in the following way. An image has been divided into a large number of square blocks by placing a square grid on it. The coordinates $(\vec{r_i})$ of these small squares covered by the image have been determined with respect to an arbitrary origin outside the structure. Then, the centre of mass $(\vec{r_m})$ of this structure has been determined. Radius of gyration has been determined with respect to this centre of mass as, $R_g^2 = \frac{1}{N}\sum_{i=1}^{N}(\vec{r_i} - \vec{r_m})^2$, where N is the number of square blocks in the image. For the smallest to the largest structure in Fig. 2, we have used $N \approx$ 300 to 2400.
[24]T. A. Witten and L. M. Sander, Phys. Rev. Lett. **47**, 1400 (1981).
[25]P. Meakin, Phys. Rev. A **27**, 1495 (1983).
[26]Z. Zhang, X. Chen, and M. G. Lagally, Phys. Rev. Lett. **73**, 1829 (1994).
[27]G. Ehrlich and F. G. Hudda, J. Chem. Phys. **44**, 1039 (1966).
[28]R. L. Schwoebel and E. J. Shipsey, J. Appl. Phys. **37**, 3682 (1966).
[29]K. Morgenstern, G. Rosenfeld, E. Lægsgaard, F. Besenbacher, and G. Comsa, Phys. Rev. Lett. **80**, 556 (1998).
[30]P. Stoltze, J. Phys.: Condens. Matter **6**, 9495 (1994).
[31]W. B. Su, S. H. Chang, W. B. Jian, C. S. Chang, L. J. Chen, and T. T. Tsong, Phys. Rev. Lett. **86**, 5116 (2001).
[32]R. Batabyal, A. H. M. Abdul Wasey, J. C. Mahato, D. Das, A. Roy, G. P. Das, and B. N. Dev, J. Appl. Phys. **113**, 034308 (2013).
[33]J. M. Gomez-Rodriguez, A. M. Baro, L. Vazquez, R. C. Salvarezza, J. M. Vara, and A. J. Arvia, J. Phys. Chem. **96**, 347 (1992).
[34]Z. Zhang and M. G. Lagally, Science **276**, 377 (1997).
[35]G. S. Bales and D. C. Chrzan, Phys. Rev. Lett. **74**, 4879 (1995).
[36]L. Esaki, Phys. Rev. **109**, 603 (1958).
[37]C. D. Geddes, A. Parfenov, D. Roll, I. Gryczynski, J. Malicka, and J. R. Lakowicz, J. Fluoresc. **13**, 267 (2003).